RSC Advances

ROYAL SOCIETY OF CHEMISTRY

www.rsc.org/advances

Cite this: DOI: 10.1039/c0xx00000x

www.rsc.org/xxxxxx

ARTICLE TYPE

Wrinkled reduced graphene oxide nanosheets for high sensitive and easy recoverable NH_3 gas detector

Su Zhang[a], Di Zhang[a], Vitaly I. Sysoev[b], Olga V. Sedelnikova[b,c], Igor P. Asanov[b,c], Mikhail V. Katkov[b,c], Huaihe Song*[a], Alexander V. Okotrub*[b,c], Lyubov G. Bulusheva[b,c], Xiaohong Chen[a]

Received (in XXX, XXX) Xth XXXXXXXXX 20XX, Accepted Xth XXXXXXXXX 20XX
DOI: 10.1039/b000000x

Highly wrinkled reduced graphene oxide nanosheets were prepared by chemical exfoliation from ball-milled graphite powder. As compared to flat reduced graphene oxide nanosheets the winkled ones showed high sensitivity and simple recovery ability when utilized as the NH_3 gas detector. According to both experimental analysis and theoretical calculation, the favourable sensing properties were attributed to a specific curved structure which allowed more strong energy change in a response process and free diffusion space for sensor recovery.

1. Introduction:

Molecular sensing of toxic substances has been extensively investigated in recent years[1]. Two-dimensional carbon allotropy of graphene and its derivatives are considered as very promising candidates for gas sensing devices due to, particularly, their excellent physicochemical properties of large specific surface area, conjugated structure with ultrahigh carrier mobility, and low noise level[2-5]. Geim and co-workers proposed that the ultimate sensitivity of graphene allows detecting a single gas molecule[6]. Aimed at high sensitive and low cost gas sensors, the previous works including both theoretical simulations[7, 8] and experimental investigations were mainly focused on modulating the intrinsic properties of graphene sheets made with various fabrication approaches such as micromechanical cleavage[6, 9, 10], epitaxial growth[11, 12], chemical vapor deposition[13, 14], and chemical or thermal reduction of graphene oxide[15-20], or modification routes such as ozone modification[21].

The morphology of graphene materials is another important influence factor for their sensing properties, but only several reports were devoted to this issue. Previously, porous graphene from steam etching of graphene oxide[22], mesh-like graphene from nanosphere lithography and ion etching[23], and three-dimensional graphene network from CVD route where nickel foam was used as both template and catalyst[24] were reported to show enhanced sensing properties towards gas molecules. However, most of the mentioned graphene sensors suffered from poor recovery ability, thus some additional assistant techniques such as thermal treatment or ultraviolet light were necessary for their secondary utilization. Noticeably, Li and coworkers reported a simple electrophoretic deposition method for the preparation of reduced graphene oxide film. This film exhibited good electrochemical sensitivity for the TNT detection. They speculated that the high performance is due to the strong interfacial accumulation abilities of graphene towards TNT molecules and high electroactive surface area due to the wrinkled structure[25].

Herein, to satisfy the demand of graphene-based sensors with high sensitivity and simple recovery ability, we designed wrinkled reduced graphene oxide nanosheets (WG) from the exfoliation of ball-milled graphite powder. The WG showed much higher sensitivity and more favourable recovery ability towards NH_3 gas compared with that of flat reduced graphene oxide nanosheets (FG). The outstanding sensing properties of WG were attributed to its highly crumpled structure according to the experimental analysis including X-ray diffraction (XRD), Raman spectroscopy, Brunauer-Emmett-Teller specific surface area, scanning electron microscopy (SEM), and high-resolution transmission electron microscopy (HRTEM), and the theoretical calculation based on density functional theory (DFT).

2. Experimental section:

2.1 Materials preparation:

The FG and WG were prepared based on the same route of solution based oxidation and thermal reduction using different graphite precursors. Natural graphite powder (Tai Chang graphite Co., Ltd., Qingdao, Shandong, 150 μm) was carried out for the preparation of FG, and the ball-milled natural graphite powder was utilized to prepare WG. Ball-milled graphite was prepared from natural graphite powder at 425 rpm ball-milling for 200 h. Ball-milling apparatus (Nanjing NanDa Instrument Plant, QM-1SP2, Planetary Ball Mill) is composed of two agate mortars. 8 of big agate balls (ca. 0.6 g/ball) and 60 of small balls (ca. 0.3 g/ball), and 0.5 g of the natural graphite powder were added in one agate mortar. The solution based oxidation was based on the modified Hummers' method, in which graphene oxide (GO) or wrinkled graphene oxide (WGO) were obtained from natural graphite and ball-milled graphite respectively. The detailed experimental pathway could be described by the following: 5 g of the graphite precursor, 2.5 g of $NaNO_3$ and 120 ml H_2SO_4 (98

wt. %) were firstly added in a 500 ml flask and stirred in an ice-water bath. 15 g of $KMnO_4$ were gradually added in the flask and kept to react at 0 ˚C for 0.5 h. Then, the temperature was raised to 35 ˚C, and the mixture left to react for 6 h. After adding excessive H_2O_2 and washing to a neutral state by deionized water, the GO or WGO dispersion was freeze-dried to produce GO or WGO powder. The FG and WG were further fabricated by thermal expansion from the as-prepared GO and WGO at 1050 ˚C during 30 s in a muffle furnace, respectively.

2.2 Methods for structural characterization

The crystal structures of the materials were measured by X-ray diffraction (XRD) recorded on a Rigaku D/max-2500B2+/PCX system operating at 40 kV and 20 mA using CuKα radiation. Raman spectroscopy was carried out using a 532 nm laser (Aramis, Jobin Yvon). The samples were prepared by dispersing in ethanol with soft sonication and dropping the dispersion on SiO_2/Si substrate followed by drying at room temperature. For each sample we measured at least 3 different points. The micro-morphologies and structures were carried out by scanning electron microscopy (SEM, JEOL, FE-JSM-6701F) and high-resolution transmission electron microscopy (HRTEM, JEOL-3010). XPS study was performed on a Phoibos 150 SPECS spectrometer using a monochromatized Al Kα radiation with the energy of 1486.7 eV. The pass energy of electron energy analyzer was set at 20 eV. The angle between the excitation beam and the entrance of the electron detector was 55º. The base pressure during the measurements was ~10–9 mBar. The binding energy scale was internally calibrated to the energy 284.4 eV of the C 1s peak. The C 1s and O 1s spectra were fitted using symmetric Gaussian/Lorentzian product function after subtraction of the background signal by Shirley's method.

2.3 Sensor preparation and test

The sensitivities of FG and WG for NH_3 detection were investigated at ambient conditions (room temperature and atmospheric pressure) by real time amperometric measurements. Firstly, FG or WG were dispersed in a toluene solution (ca. 0.01 mg/ml) by soft sonication and subsequently deposited on SiO_2/Si substrate (ca. 5 mm* 5 mm) by spin coating to obtain thin films. A sample with silver contacts on a teflon cell with gold terminals was sealed in a chamber with a volume of 25 mL having two gas flow connectors (input and output). The measurements of the sensing properties of as-prepared sensor devices were carried out with a picoammeter KEITLHLY 6485 by registering the current with DC voltage of 1 V applied to the samples. A standard test cycle comprises two main steps which include (1) exposure mixture of argon and NH_3 for response registration and (2) exposure pure argon for recovery of the sensor to its initial state. The schematic of the testing equipment was given in the Supporting Information.

3. Results and discussion

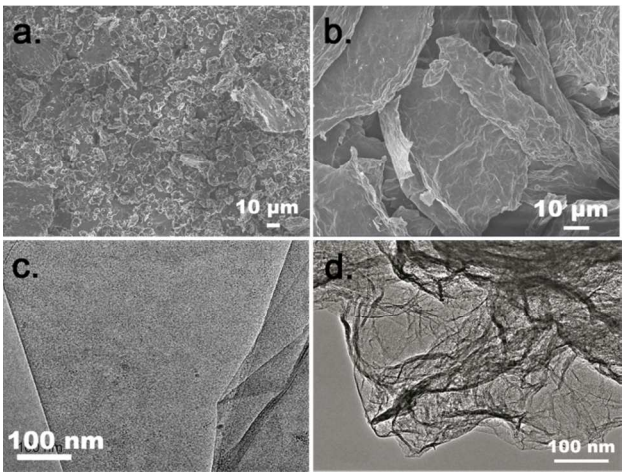

Figure 1 SEM images of (a) ball-milled graphite and (b) WG, HRTEM images of (c) FG and (d) WG.

The micro-morphologies of the as-prepared products are given in Figure 1. Both of WG and FG show thin layer silk like morphology, but the WG (Figure 1b and d) demonstrates much higher curved and twisted features than that of the FG (Figure 1c).

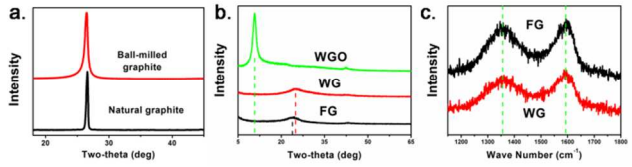

Figure 2 XRD patterns of (a) natural graphite and ball-milled graphite powder (b) WGO and WG and FG. (c) Raman spectra of FG and WG.

According to the previous reports, flat graphite platelets can transform to highly curved structures by mechanical shear and impact during ball-milling[26, 27]. In the XRD patterns of ball-milled graphite powder given in Figure 2a, the broadening of the (002) peak (ca. 26 °) compared with that of natural graphite indicates disordering of the graphite structure[28].The XRD patterns of the products are given in Figure 2b. The stacking peak of the as-prepared WGO appears at low degree of ca. 10.75˚, indicating that the synergistic effect of intercalation and oxidation is sufficiently taken place in ball-milled graphite, therefore a large amount of oxygen-containing functional groups is introduced into the interlayer space during chemical oxidation[29, 30]. Noticeably, only a wide and dispersive peak can be observed in the XRD patterns of WG and FG, suggesting GO and WGO are easily exfoliated to thin layer graphenes by rapid thermal expansion[30, 31]. Carried out by N_2 adsorption-desorption technique, the FG performs larger specific surface area of 648 $m^2 g^{-1}$ than 358 $m^2 g^{-1}$ of the WG. This can be attributed to the compact layer stacking structure in the curved regions of WG flakes, which is observed from the small but perceivable peak position difference between WG and FG in the XRD patterns.

From Raman spectra shown in Figure 2c, these two graphene materials have almost the same defect density[32]. Besides, measured by X-ray photoelectron spectroscopy and Fourier transform infrared spectroscopy (Seeing in the SI), the as-prepared FG and WG exhibited almost the same chemical components as well as functional group distributions.

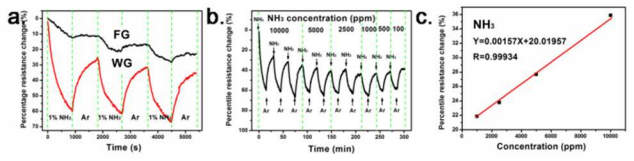

Figure 3 (a) sensing properties of WG and FG in 1% NH_3, (b) sensing property of WG under different NH_3 concentrations and (c) the linear relationship between resistance change and concentration.

Figure 3 shows the sensing performance of the FG and WG. The response is calculated as the percentage of resistance change during real-time testing. The WG exhibits more than 3 times response intensity (ca. 35 %) and much better recovery ability compared with that of FG (ca. 10 %) when exposed in 1 % NH_3 atmosphere (Figure 3a). After exposed in argon atmosphere for 15 min, the resistance recovery of WG in each cycle is more than 85 %, while only ca. 40 % of recovery can be observed for FG. Even under the low concentration of 100 ppm the WG shows the sensing response of 17 % (Figure 2b), and it can be fully recovered after the initial several cycles. The response to concentration of WG for NH_3 gas follows a linear relationship ranging from 1000 ppm to 10000 ppm (Figure 3c).

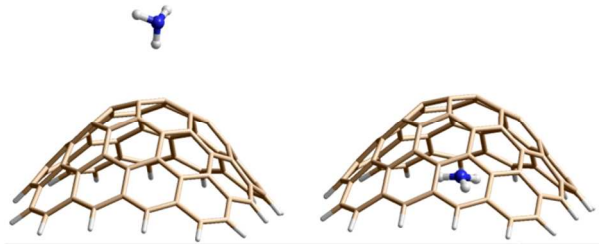

Figure 4 Energy favorable configuration of NH_3 adsorbed on the positive (a) and negative (b) curved graphene surface.

From the above discussion, FG exhibits almost two times larger specific surface area than that of WG, while both of them have much similar defect density and chemical composition. In this case, the remarkable sensing properties of WG are mainly attributed to its highly wrinkled structure. To check this statement, computer simulations of NH_3 adsorption on the models of FG and WG were carried out at the B3LYP-D3/6-31G*+ level. The model of WG was proposed by removing a part of carbon atoms from the graphene lattice. Small-size vacancies formed as the result of such process can be reconstructed in topological defects. Considering that the most preferable defects are pentagonal rings we introduced a pair of pentagons in a graphene fragment and geometry relaxation produced a cockleboat structure. Adsorption of a NH_3 molecule was studied on the positively and negatively curved surface of the cockleboat structure. Figure 4 shows the most thermodynamically preferable configurations of the adsorbed molecule. In case of the positive curvature, NH_3 interacts with the surface through a hydrogen atom (Fig. 4a) similar to the adsorption position for the flat graphene fragment. The calculated adsorption energy is -0.10 eV for the former model and -0.17 eV for the latter one. In case of the negative curvature, NH_3 oriented by nitrogen atom to the surface (Fig. 4b) with an adsorption energy of -0.31 eV. Such NH_3 configurations indicate the induction of negative and positive charge respectively on the convex and concave graphene surface. The charge transfer between molecule and graphene fragment is quite weak (not more than 0.05e) for all models evidencing the physical adsorption nature of NH_3 on graphene flakes.

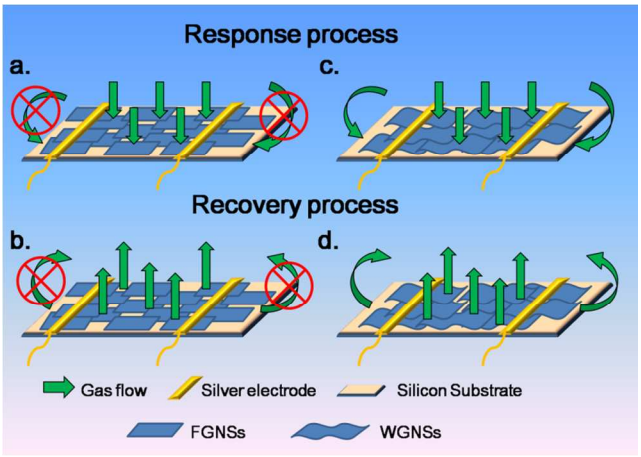

Figure 5 Schematic of the sensing procedures of FG and WG.

The recover ability of graphene gas sensors is based on the desorption rate[18]. It can be assumed that the poor recovery ability of FG is due to the slow diffusion of gas molecules which absorbed between the flat graphene platelets and the substrate[18, 33] because the physical absorbed gas molecules on the top layer of the graphene can be easily removed during exposed in argon (Figure 5a and c). However, the highly corrugated structure of WG can provide more free space (Figure 5b and d), which allows the fast diffusion of the absorbed gas molecules[34], thus favoring the recovery ability.

4. Conclusion

A special highly wrinkled structure of graphene nanosheets was achieved by chemical exfoliation of the ball-milled graphite powder. When utilized for gas sensing, WG exhibited a much higher sensitivity and favourable recovery ability compared with that of FG. From the experimental and simulation results, the excellent sensing properties were attributed to the wrinkled structure which provides intensive adsorption energy change and free space to facilitate gas diffusion.

ACKNOWLEDGMENTS

Dr. Su Zhang, Dr. Di Zhang, Prof. Huaihe Song and Prof. Xiaohong Chen thank the financial support from the National Natural Science Foundation of China (51202009 and 51272016).

Prof. Alexander Okotrub, Prof. Lyubov Bulusheva and Dr. Igor Asanov thank the financial support from the Russian Foundation of Basic Research (14-03-91156 and 13-03-90919).

Notes and references

[a] *State Key Laboratory of Chemical Resource Engineering, Beijing Key Laboratory of Electrochemical Process and Technology for Materials, Beijing University of Chemical Technology, Beijing, 100029, P. R. China.*

[b] Nikolaev Institute of Inorganic Chemistry SB RAS, 3 Acad. Lavrentiev Ave., 630090, Novosibirsk, Russian Federation.
[C] Novosibirsk State University, 2 Pirogov Str., 630090, Novosibirsk, Russian Federation.

*Corresponding Authors:
Prof. Huaihe Song, E-mail: songhh@mail.buct.edu.cn; Fax/Tel: +86-010-6443-4916
Prof. Alexander V. Okotrub, E-mail: spectrum@niic.nsc.ru; Fax/Tel: +7-383-330-53-52

† Electronic Supplementary Information (ESI) available: See DOI: 10.1039/b000000x/

1 S. Capone, A. Forleo, L. Francioso, R. Rella, P. Siciliano, J. Spadavecchia, D. Presicce and A. Taurino, J. Optoelect. Adv. Mater., 2003, 5, 1335-1348.
2 W. Yuan and G. Shi, J. Mater. Chem. A., 2013, 1, 10078-10091.
3 F. Yavari and N. Koratkar, J. Phys. Chem. Lett., 2012, 3, 1746-1753.
4 Y. Liu, X. Dong and P. Chen, Chem. Soc. Rev., 2012, 41, 2283-2307.
5 K. R. Ratinac, W. Yang, S. P. Ringer and F. Braet, Environ. Sci. Technol., 2010, 44, 1167-1176.
6 F. Schedin, A. Geim, S. Morozov, E. Hill, P. Blake, M. Katsnelson and K. Novoselov, Nat. Mater., 2007, 6, 652-655.
7 B. Huang, Z. Li, Z. Liu, G. Zhou, S. Hao, J. Wu, B.-L. Gu and W. Duan, J. Phys. Chem. C., 2008, 112, 13442-13446.
8 Y.-H. Zhang, Y.-B. Chen, K.-G. Zhou, C.-H. Liu, J. Zeng, H.-L. Zhang and Y. Peng, Nanotechnology, 2009, 20, 185504.
9 S. Rumyantsev, G. Liu, M. S. Shur, R. A. Potyrailo and A. A. Balandin, Nano Lett., 2012, 12, 2294-2298.
10 Y. Dan, Y. Lu, N. J. Kybert, Z. Luo and A. C. Johnson, Nano Lett., 2009, 9, 1472-1475.
11 R. Pearce, T. Iakimov, M. Andersson, L. Hultman, A. L. Spetz and R. Yakimova, Sensor. Actuat. B. Chem., 2011, 155, 451-455.
12 M. W. Nomani, R. Shishir, M. Qazi, D. Diwan, V. Shields, M. Spencer, G. S. Tompa, N. M. Sbrockey and G. Koley, Sensor. Actuat. B. Chem., 2010, 150, 301-307.
13 M. Gautam and A. H. Jayatissa, Mat. Sci. Eng. C., 2011, 31, 1405-1411.
14 F. Yavari, E. Castillo, H. Gullapalli, P. M. Ajayan and N. Koratkar, Appl. Phys. Lett., 2012, 100, 203120.
15 J. D. Fowler, M. J. Allen, V. C. Tung, Y. Yang, R. B. Kaner and B. H. Weiller, ACS Nano, 2009, 3, 301-306.
16 G. Lu, L. E. Ocola and J. Chen, Nanotechnology, 2009, 20, 445502.
17 G. Lu, L. E. Ocola and J. Chen, Appl. Phys. Lett., 2009, 94, 083111.
18 J. T. Robinson, F. K. Perkins, E. S. Snow, Z. Wei and P. E. Sheehan, Nano Lett., 2008, 8, 3137-3140.
19 G. Lu, S. Park, K. Yu, R. S. Ruoff, L. E. Ocola, D. Rosenmann and J. Chen, ACS Nano, 2011, 5, 1154-1164.
20 V. Dua, S. P. Surwade, S. Ammu, S. R. Agnihotra, S. Jain, K. E. Roberts, S. Park, R. S. Ruoff and S. K. Manohar, Angew. Chem. Int. Ed., 2010, 49, 2154-2157.
21 M. G. Chung, D. H. Kim, H. M. Lee, T. Kim, J. H. Choi, J.-B. Yoo, S.-H. Hong, T. J. Kang and Y. H. Kim, Sensor. Actuat. B. Chem., 2012, 166, 172-176.
22 T. H. Han, Y.-K. Huang, A. T. Tan, V. P. Dravid and J. Huang, J. Am. Chem. Soc., 2011, 133, 15264-15267.
23 R. K. Paul, S. Badhulika, N. M. Saucedo and A. Mulchandani, Anal. Chem., 2012, 84, 8171-8178.
24 F. Yavari, Z. Chen, A. V. Thomas, W. Ren, H.-M. Cheng and N. Koratkar, Sci. Rep., 2011, 1, 1-5.
25 L. Tang, H. Feng, J. Cheng and J. Li, Chem. Commun., 2010, 46, 5882-5884.
26 X. Chen, H. Yang, G. Wu, M. Wang, F. Deng, X. Zhang, J. Peng and W. Li, J. Cryst. Growth, 2000, 218, 57-61.
27 J. Huang, H. Yasuda and H. Mori, Chem. Phys. Lett., 1999, 303, 130-134.
28 J. Huang, Acta. Mater., 1999, 47, 1801-1808.
29 S. Zhang, L. Zhu, H. Song, X. Chen, B. Wu, J. Zhou and F. Wang, J. Mater. Chem., 2012, 22, 22150-22154.
30 S. Zhang, J. Niu, H. Song, L. Zhu, J. Zhou, X. Chen, J. Liu, S. Hong and R. Song, J. Mater. Chem. A., 2013, 1, 14103-14107.
31 M. J. McAllister, J.-L. Li, D. H. Adamson, H. C. Schniepp, A. A. Abdala, J. Liu, M. Herrera-Alonso, D. L. Milius, R. Car and R. K. Prud'homme, Chem. Mater., 2007, 19, 4396-4404.
32 E. Barros, N. Demir, A. Souza Filho, J. Mendes Filho, A. Jorio, G. Dresselhaus and M. Dresselhaus, Phys. Rev. B., 2005, 71, 165422.
33 H. E. Romero, P. Joshi, A. K. Gupta, H. R. Gutierrez, M. W. Cole, S. A. Tadigadapa and P. C. Eklund, Nanotechnology, 2009, 20, 245501.
34 Q. Ji, I. Honma, S. M. Paek, M. Akada, J. P. Hill, A. Vinu and K. Ariga, Angew. Chem., 2010, 122, 9931-9933.